From binary breakup to multifragmentation: Computer simulation

David H. Boal and James N. Glosli
Department of Physics, Simon Fraser University, Burnaby, British Columbia, Canada V5A 1S6
(Received 27 July 1987)

A semiclassical model developed for the computer simulation of nuclear reactions is applied to the problem of fragmentation in proton and heavy ion induced reactions. Simulations based on the model are used to follow the time evolution of the reactions in both coordinate and phase space as well as to calculate correlations for quantities such as fragment positions and masses. Three reactions are selected for detailed study: p+Ag at 300 MeV, and Ca+Ca at 25 and 50 MeV/nucleon bombarding energy. It is shown that the behavior expected for these reactions from the mechanical instability properties of nuclear matter is supported by the simulations. An experimental measure of the change from binary breakup to multifragmentation is shown to be the two-particle correlation function in mass.

I. INTRODUCTION

Numerical simulation techniques have been applied to nuclear physics problems for about four decades. Several approaches have been developed, each with its own area of applicability (for a general review see Ref. 1). The methods range from the cascade model, which solves the classical A-body problem,[2] through Boltzmann-like equations for the evolution of one-body distributions,[3,4] to the solution of the hydrodynamic equations for integrated quantities such as the energy and baryon number densities.[5] The study of nuclear fragmentation requires elements from many of these approaches: one needs the A-body nature of the cascade approach as well as the nuclear binding and Pauli blocking effects which have been incorporated in the Boltzmann-like approaches. Recently, we developed a semiclassical model[6,7] (see also Refs. 8–10) in which the nucleon equations of motion are integrated classically while effects arising from Fermi-Dirac statistics are incorporated through a collision term which evaluates the occupancy of phase space available to colliding nucleons.

In our previous work,[6] the model was applied to reactions at energies in the 100 MeV/nucleon range and was used to develop a description of the reaction mechanism at these energies. Here, we will concentrate on the physics of the nuclear matter liquid-gas phase transition and its effect on the production of fragments in intermediate energy nuclear reactions. In Sec. II, the basis of the simulation which will be used in attacking these questions is outlined, and an intuitive picture of intermediate energy reactions is developed by showing the predicted time evolution of three selected central collisions: p+Ag at 300 MeV, Ca+Ca at 25 and 50 MeV/nucleon. The features of the reactions as seen in experiment are dealt with in Sec. III, namely the energy spectra and the isotopic yields. Section IV contains results from the study of reaction trajectories in phase and coordinate space. It is demonstrated that phase-transition-like effects are observable in the trajectories, although the relationship between these effects and those expected in infinite neutral nuclear matter is not yet clear. A summary is contained in Sec. V.

II. A MODEL FOR FRAGMENTATION

The model[6] which we wish to use to investigate fragmentation phenomena is one based on classical mechanics. The individual nucleons are assigned positions and momenta which are updated at finite time intervals. The force to which the nucleons are subjected is obtained from the Coulomb interaction and a density dependent mean field which has the form

$$U(\rho)=a\left[\frac{\rho}{\rho_0}\right]+b\left[\frac{\rho}{\rho_0}\right]^2+c\epsilon_i\frac{\rho_p-\rho_n}{\rho_0}\ . \tag{2.1}$$

The parameters a, b, and c are assigned the values -124, 70.5, and 25 MeV. Normal nuclear matter density is denoted by ρ_0 (equal to 0.17 fm^{-3} here) while the individual proton and neutron densities are denoted by ρ_p and ρ_n. The quantity ϵ_i is equal to $+1$ (-1) for protons (neutrons). Unlike one-body kinetic equations such as the Boltzmann or Vlasov equations, here we wish to keep the fluctuations and simulate the dynamics on an event-by-event basis. Clearly, point nucleons are not appropriate mathematically (or appropriate physically) for the evaluation of densities when there are so few particles in the system. Hence, for the purpose of evaluating a nucleon's density in coordinate and phase space, its probability density will spread out with a Gaussian function

$$\exp\left\{-\left[(\alpha\Delta r)^2+\left[\frac{\Delta p}{\alpha}\right]^2\right]\right\}, \tag{2.2}$$

where Δr and Δp are the differences in position and momentum between the classically assigned values of a given nucleon and the point in phase space at which the density is to be evaluated. The parameter α is determined by demanding that phase space is as close to the saturation value as possible for a cold nucleus (this gives $\alpha=0.5$ fm^{-1}). The nuclear potential at any given posi-

 ©1988 The American Physical Society

tion can be evaluated by determining the nuclear density at that position by summing over the Gaussian density distributions of all nucleons.

In the model, individual nucleons are also allowed to scatter from each other in a manner similar to the Boltzmann collision term. The scattering is handled stochastically; at the distance of closest approach, a pair of nucleons scatter into new momenta chosen randomly from a predetermined distribution in angle. At these energies, the scattering is isotropic in the center-of-mass frame. The magnitude of the NN cross section is taken from the experimental data in the 100–300 MeV bombarding energy range where the cross section is observed to be constant. The rise in the cross section at low momentum (where the cross section goes like p^{-2}) is assumed to be included in the attractive part of the nuclear mean field. The scattering process provides a mechanism for the incorporation of the Pauli exclusion principle in the Uehling-Uhlenbeck sense; once the new momenta for the members of the scattering pair are chosen, the fractional occupancy of the new points in phase space (f_1 and f_2) is checked. A random number is chosen and compared to

$$u=(1-f_1)(1-f_2)\ . \tag{2.3}$$

The collision is allowed or forbidden according to the value of the random number chosen. To the extent that the collisions are fast, this technique can be used to mimic the Pauli exclusion principle and keep nucleons from moving too far into regions of phase space which are forbidden.

The calculational technique of the model bears close resemblance to that of the Boltzmann-like equations used to solve for the time evolution of one-body distributions of fermions. Hence, an average over the individual events generated by the model should yield similar results to those found from the corresponding kinetic equation. However, in this model there will be small artificial inhomogeneities in phase space occupancy which are associated with representing the nucleon wave functions by single Gaussians (a coarse grained spatial average will approach the correct density, as expected). These fluctuations will limit the model's ability to describe some aspects of low energy reactions or processes which involve excitation energies of a few MeV per nucleon. Similarly, because the collision term is the only way Fermi-Dirac statistics are incorporated in the model, the existence of small local fluctuations in phase space implies that there is a small, but finite, probability that a pair of nucleons can scatter even though they lie in regions of phase space which, on average, are saturated. Thus, over long time there will be "artificial" evaporation of nucleons and the model is not appropriate for the evaluation of evaporation-like processes. Of course, kinetic equations are not generally applied to the study of evaporation processes because each event would have to be followed for a prohibitively large number of time steps.

Bearing these caveats in mind, we now attempt to develop an intuitive picture for the reaction mechanisms of proton and heavy ion induced reactions at intermediate energy. All collisions to be discussed are at zero impact parameter. The first reaction of interest is p + Ag at 300 MeV. The coordinate space positions of the nucleons in a single collision are shown in Fig. 1. The event is shown at three time steps: 1, 100, and 150 fm/c. In this particular event, the incoming proton has been stopped in the target and its energy has become distributed among the target nucleons (this is not always the case in central collisions of proton induced reactions and is even less likely in peripheral ones). Although it cannot be seen from the figure, the target is observed to oscillate in time, and finally begin to break apart on the time scale of hundreds of fm/c.

The central collision of two calcium nuclei at a bombarding energy of 25 MeV/nucleon is a more energetic process, as is evidenced by Fig. 2. One can see that a fused system is formed, although it has a high excitation energy and breaks up on a shorter time scale than does the p + Ag system. Moreover, if one raises the bombarding energy further to 50 MeV/nucleon, breakup is both rapid and extensive. This is illustrated in Fig. 3. As the energy is raised beyond 50 MeV/nucleon, destruction of the nuclei becomes more complete in central collisions, particularly at bombarding energies beyond 100 MeV/nucleon (reactions whose energies are high enough to lead to vaporization will be dealt with in a subsequent paper). We will use three reactions, then, as representational of the change from binary-breakup–like decay to multifragmentation. In the center-of-mass frame, the total kinetic energy per nucleon is about 3, 6, and 12 MeV for Figs. 1–3, respectively.

As will be emphasized in Sec. IV, the simulations show that in multifragmentation reactions, the fluctuations which develop early in the reaction are propagated through the expansion regime and emerge as fragments as the reaction zone goes out of equilibrium. The simulations do not show the formation of a hot gas from which fragments coalesce late in the reaction. It is also clear that the nuclear surface tension plays a strong role in fragmentation at all of the energies considered.

III. KINETIC TEMPERATURES AND ISOTOPIC YIELDS

Before proceeding to investigate the time evolution of the reactions, the simulations will be used to extract a few quantities which can be accessed experimentally. These predictions are currently of limited use since they are at fixed impact parameter; however, it should be checked that their values are in the range expected from impact parameter averaged data. For this section, and Secs. IV B and IV C a total of 800 events were complied for each reaction. Each event spanned a time frame of 150 fm/c, at the end of which the nucleons were assigned to fragments according to a minimum separation technique.[6]

The first quantity of interest is the distribution of isotopic yields of light fragments. These are shown in Fig. 4 for each of the chosen reactions. All of the distributions show a rapid falloff as one moves away from the $N=Z$. line. This is a result both of the isospin depen-

dent interaction in the mean field and of the combinatorics of choosing a given fragment Z and N from the parent system. In any event, were one to do a fit to these yields with a chemical equilibrium model containing a "chemical" temperature as a parameter, a low temperature would be obtained. Comparing one reaction type with another, one can see that the yields fall much more rapidly with increasing mass in the proton induced reaction than they do in the other reactions. Further, from both the width of the distribution around $N=Z$ and the falloff with mass, it can be seen that the chemical temperature is increasing with excitation energy of the system, as one would expect. Lastly, it should be mentioned that the yields typically agree with the data at the factor of two level (detailed comparison of the predicted yields with data is difficult since the model

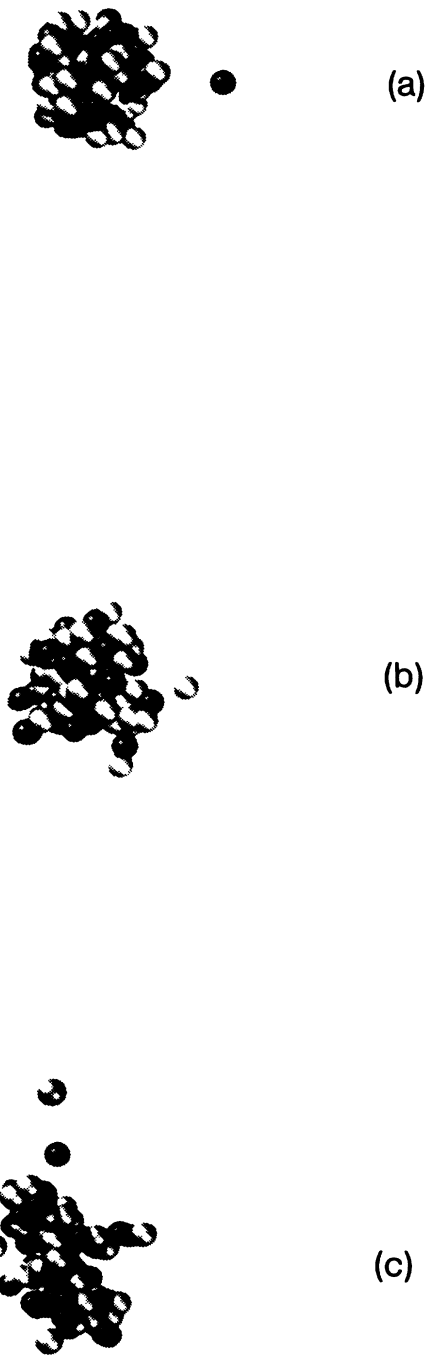

FIG. 1. Time evolution of a central p + Ag collision at 300 MeV bombarding energy. The reaction is shown at 1, 100, and 150 fm/c elapsed time. The solid spheres represent protons while the open ones are neutrons.

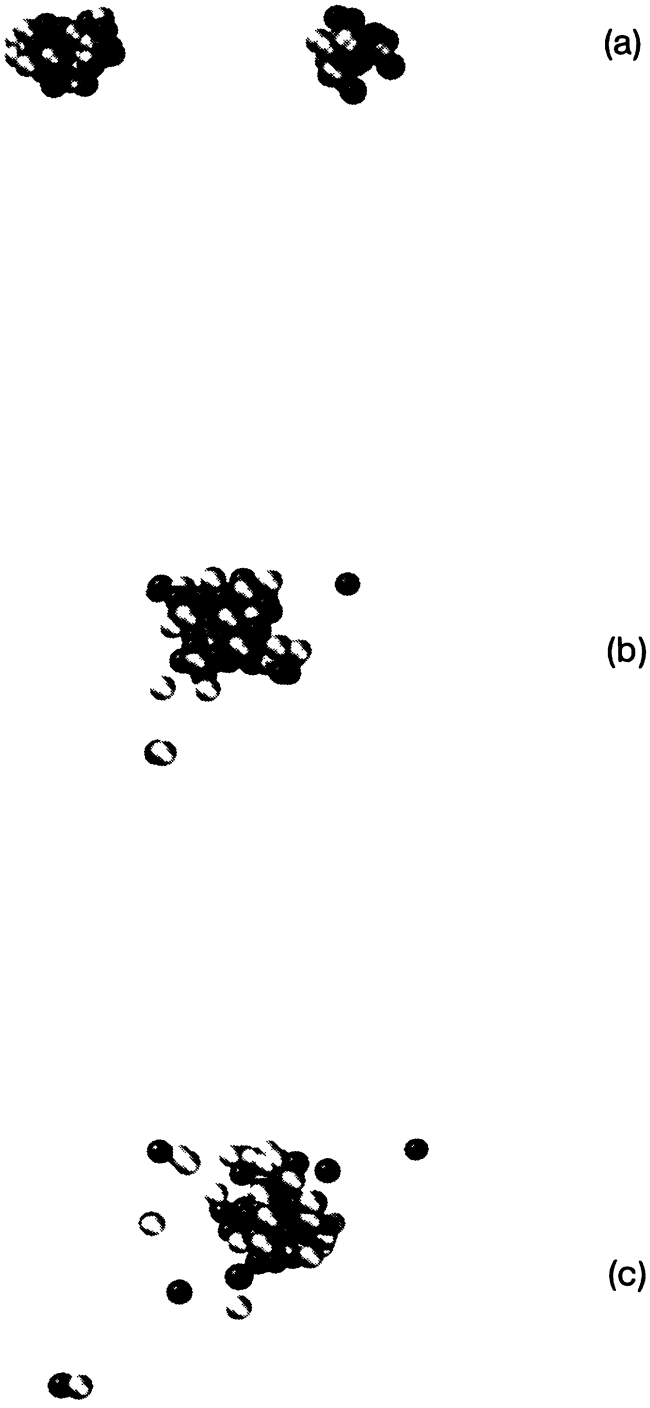

FIG. 2. Time evolution of a central Ca + Ca collision at 25 MeV/nucleon bombarding energy. Same representation as Fig. 1.

cannot be expected to produce fragments with the correct binding energy, particularly for light fragments).

The behavior of the kinetic temperature, as opposed to the chemical temperature, can be found from the energy spectra. We show in Fig. 5 the differential multiplicity for nucleon emission in the center of mass frame for the three reactions. For each reaction, the energy spectra are presented for three angles in the center-of-mass (c.m.) frame: 10°, 90°, and 170° (the bin size being 20°). Within the statistics, the slopes of the spectra are observed to decrease as the amount of energy available for thermalization increases. However, the distributions are not isotropic in the c.m. frame (particularly the proton induced reactions) and so we have not attempted to extract a kinetic temperature.

The behavior of the yields and energy spectra is qualitatively what is expected from impact parameter aver-

FIG. 3. Time evolution of a central Ca + Ca collision at 50 MeV/nuclon bombarding energy. Same representation as Fig. 1.

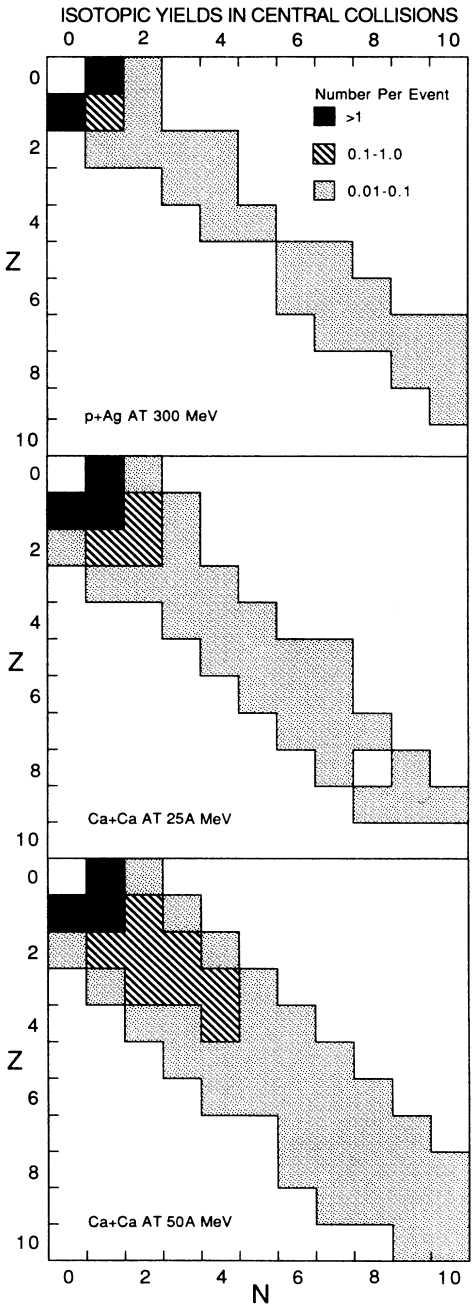

FIG. 4. Isotopic yields in the light to medium mass fragment range for the reactions shown in Figs. 1–3. The yields are given as the number of fragments of a given Z,N per event.

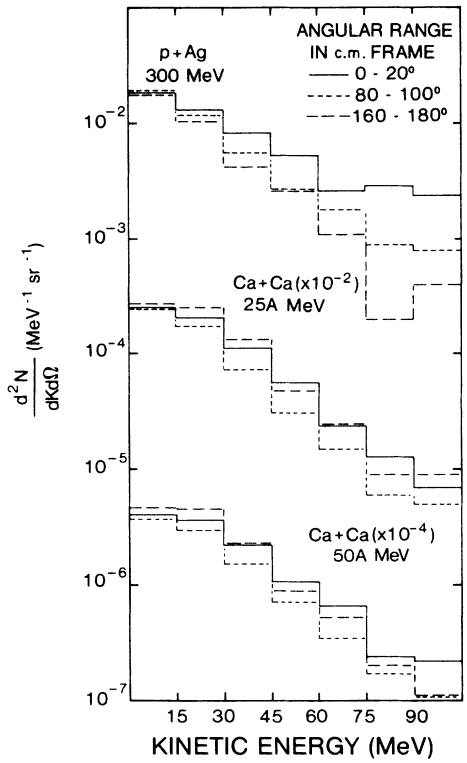

FIG. 5. Nucleon energy spectra for the reactions in Figs. 1–3. The spectra are shown at three angles in the c.m. frame: 0°–20°, 80°–100°, and 160°–180°.

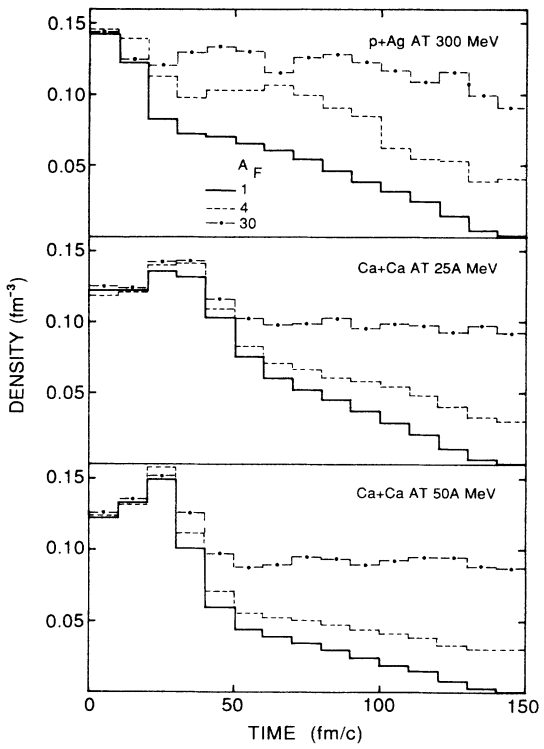

FIG. 6. Time evolution of the average local coordinate space density in the vicinity of nucleons which finally emerge from the reaction as free nucleons ($A=1$) or in bound clusters ($A=4,30$). Results are shown for the reactions in Figs. 1–3.

aged data. In applications at higher energies,[6] the agreement of the model and data was typically within a factor of 2.

IV. REACTION TRAJECTORIES

A. General features

To put the qualitative features of the reaction mechanisms developed in Sec. II on a more quantitative basis, the simulations will be used to determine the time evolution of the reaction trajectory in coordinate and phase space. The method is the following: During each event of the simulation, the positions and momenta of each nucleon are stored every 10 fm/c in time. At the end of the event, a cluster search is performed and it is determined which cluster, if any, each nucleon belongs to (where the clusters are defined by the minimum separation criterion; see Ref. 6). By tracing back through the stored positions and momenta, the local coordinate and phase space density through which each nucleon passed on its way through the reaction can be determined. Averaging over many events, one can determine the average local densities traversed by nucleons which ultimately emerge in a given cluster mass. For this subsection, the event sample contains 250 events for the proton induced reaction and 700 events for each of the calcium reactions.

The time evolution of the average coordinate space density is shown in Fig. 6 for the reactions of Figs. 1–3. Three sample cluster masses are shown: $A=1$, 4, and 30. First, some general comments on the figure. In the proton induced reaction, one observes that the falloff of the density with time is slower than what is observed for the heavy ion reactions. Intuitively, we would expect that with such a low excitation energy, the processes in this reaction would be very slow compared to the heavy ion reactions, as was pointed out earlier in the discussion of Figs. 1–3. Further, it would appear that the density falls off more slowly as the charge of the emitted fragment increases, which would be expected because of the Coulomb barrier. This interpretation can be strengthened by determining an "emission time" for each fragment and comparing emission rates between fragment masses.

The emission time in these simulations is defined as the first time step (as measured in 10 fm/c steps) at which the aveage local density observed by nucleons which ultimately emerge as the fragment falls below 0.08 fm^{-3}. While this choice is a little arbitrary, it will do for our purposes here. With this definition of the emission time, an emission rate can be calculated (the time evolution of this quantity is shown in Fig. 7 for nucleons and $A=4$ fragments). Fragments with lower charge tend to be emitted earlier in the reaction than those with larger charges, and, since nucleons are more copiously produced than fragments, their emission rate is higher. Since Fig. 7 is plotted logarithmically, the time dependence of the emission rate has the usual exponential form. Taking the slope one can assign a lifetime to the

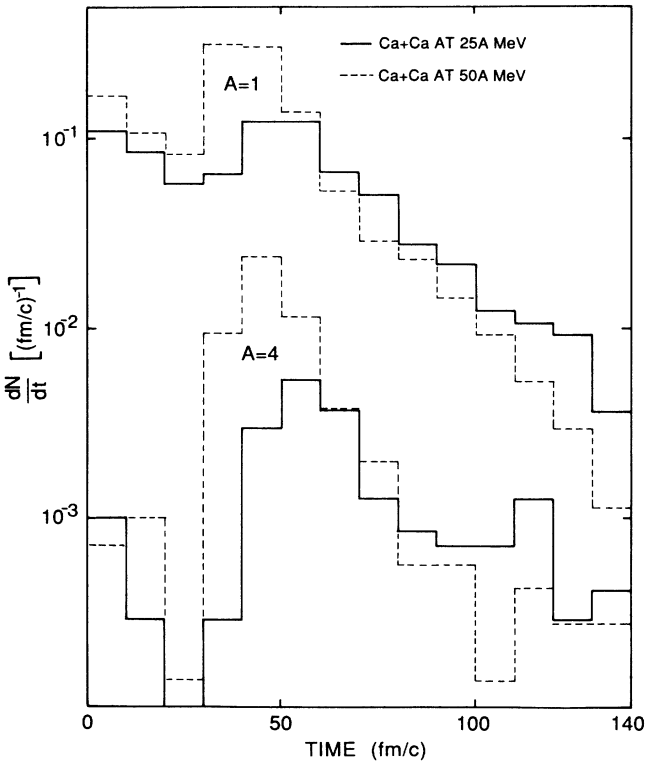

FIG. 7. "Emission rate" of nucleons and $A=4$ clusters in the reactions shown in Figs. 2 and 3. In the simulation, the emission time is defined as the time when the average local coordinate space density observed by nucleons in a cluster first drops below 0.08 fm.$^{-3}$.

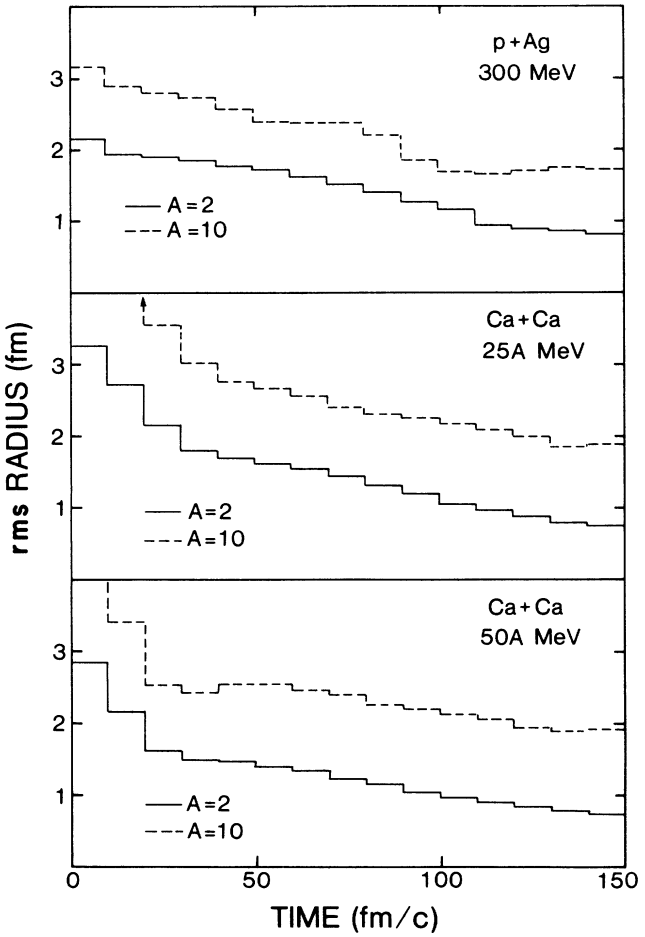

FIG. 8. Time evolution of root mean square radius of fragments with mass 2 and 10 for the reactions shown in Figs. 1–3.

emission process of about 10^{-22} s. This time scale is characteristic of preequilibrium emission from highly excited systems.[11] Longer time scale evaporative processes will not be visible in the simulations because the time evolution of the systems was stopped at 150 fm/c.

Although the emission rate indicates that the process is fairly rapid, to learn more details about the mechanism more exclusive probes of the simulations must be used. For example, an important question is at what point do the nucleons which emerge as a cluster become correlated in their motion? In long time scale processes, one might expect that nucleons have relatively uncorrelated motion until they form a cluster near the nuclear surface and have a reasonable chance of escaping. In short time scale processes, correlations in their motion may develop much earlier on. Determining which of these two scenarios is more important in a given excitation energy range is not without ambiguity, since clusters may repeatedly form and dissolve during the reaction. The method which will be used here is to determine the rms radius of the cluster (defined by the nucleons which emerge in the cluster at large times) and follow its temporal evolution. The results are plotted in Fig. 8 for two fragment masses, 2 and 10.

The top part of the figure shows the results for the proton induced reaction. There, the initial rms radius of what ultimately emerges as an $A=10$ system is large, comparable to, but smaller than, the rms radius of the target nucleus. The rms radius of the two particle pairs which ultimately emerge as $A=2$ fragments is smaller, although still much larger than the pn bound state of the simulation. This is partly because in the simulations, the nucleons are prevented from coming too close to each other by equation of state and collision effects, so that a weak correlation in their motion is present. However, both results are in agreement with what one expects for long time scale processes: If a fragment were ejected from the nucleus during the short transit time of the projectile, then the initial rms radius of the fragment would be not far from its asymtotic value.

The proton induced reaction shows what happens for a relatively cold system. The 25 MeV/nucleon Ca + Ca system shows what to expect from a more fusionlike process. First, it can be seen that the initial average radii are substantially larger in the fusionlike reaction, and for many fragements, actually exceed the rms radius of the calcium nucleus considerably. This reflects the fact that a given fragment may have nucleons which originated in either parent calcium. The effect is stronger for the heavier fragments. Additionally, the rms radius of the light system does not show a decrease which is any more rapid than the heavy fragments; again, this is consistent

with the system fusing.

The lower part of the figure is for the 50 MeV/nucleon Ca + Ca reaction. It is noticeable that the initial radii are distinctly lower than those observed in the 25 MeV/nucleon reaction. This is expected because the fusion process is much less complete. At higher energies nuclei have a greater tendency to simply break apart during the reaction because of the shorter time scale. This tends to support the claim made in Sec. II that the density fluctuations formed early in the reaction are propagated through it. Just as was observed in Fig. 6 for the average coordinate space density, the rms radii do not support a description of fragment formation in which the density drops to very low values and the clusters condense at late times.

B. Trajectories in the mechanical instability region

For nuclear reactions, one of the more important features of the nuclear matter phase diagram is the mechanical instability region.[12] The temperatures and densities of the boundary of this region are illustrated by Fig. 9. In the figure, the liquid-gas coexistence curve is labeled by LGC while the isothermal and isentropic spinodal curves [defined by $(\partial P/\partial\rho)_T=0$ and $(\partial P/\partial\rho)_S=0$, respectively] are labeled by ITS and IES. Also shown in the figure are curves of constant entropy.

The boundaries of the phase diagram are not particularly sensitive to the specific choice of parametrization of the nucleon-nucleon interaction; rather similar results were obtained[13,14] by using different parametrizations. However, the inclusion of the Coulomb interaction and other effects lowers the predicted value of the critical temperature considerably.[15]

For the reaction mechanism, the implications of the existence of the mechanical instability region are the following: At low excitation energies, a system will not be able to reach the spinodal curve. Consequently, it will simply oscillate in density and slowly lose particles by evaporation. At higher energies, a system may be able to enter the region and the subsequent growth of density fluctuations will lead to its breakup. At higher energies still, the system will vaporize.

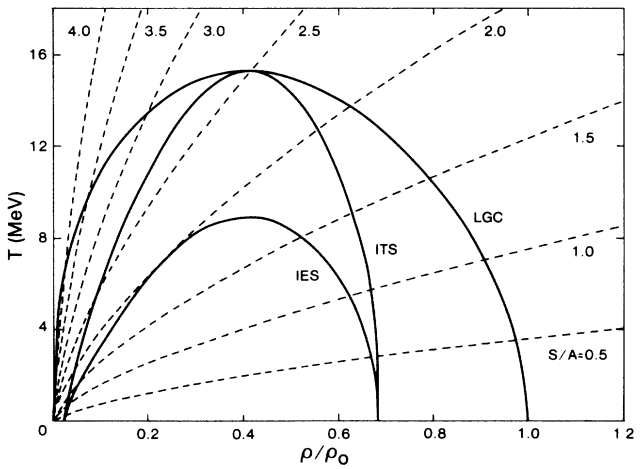

FIG. 9. Phase diagram of neutral nuclear matter associated with a zero range Skyrme-type interaction. Isentropes of given values of the entropy per nucleon (S/A) are shown by the dashed curves. The liquid-gas coexistence curve is labeled as LGC; the isothermal and isentropic spinodals are labeled as ITS and IES, respectively (from Ref. 13).

To assess whether the properties of the phase diagram are even relevant to a discussion of the reaction products, it should be checked to ensure that the interaction underlying the phase diagram (long range attraction and short range repulsion) manifests itself in those reaction products. One useful method is to examine the two particle correlation function in coordinate space $C(\mathbf{r}_1,\mathbf{r}_2)$. We define this via

$$C(\mathbf{r}_1,\mathbf{r}_2)=N_0\frac{N(\mathbf{r}_1,\mathbf{r}_2)}{N(\mathbf{r}_1)N(\mathbf{r}_2)}\ , \tag{4.1}$$

where $N(\mathbf{r}_1,\mathbf{r}_2)$ is the number of coincident pairs of nucleons at positions $\mathbf{r}_1$ and $\mathbf{r}_2$, while $N(\mathbf{r})$ is the total number of nucleons at position $\mathbf{r}$. There is an overall normalization factor N_0 to ensure that $C(\mathbf{r}_1,\mathbf{r}_2)$ goes to unity as Δr goes to infinity. In numerical simulations, the nucleon positions are, of course, segregated into finite bins in coordinate space for analysis purposes. It is more convenient to replace the denominator in Eq. (4.1) by a number of pairs generated by randomly choosing nucleons from different events. This event mixing technique allows one to avoid many of the difficulties imposed by having to match up bin sizes in the numerator and denominator.

What one would expect to see is a suppression of the correlation function at small relative separation arising from the short range repulsion, and then a strong enhancement at separations typical of the average internucleon separation in the liquid drops. At larger separations, there again should be a suppression of the correlation function, since nucleons slightly outside the drop's surface should be pulled inside by the nuclear force (or repelled by the charge, if they are charged or are residing in other charged drops). The results for two of the reactions considered in the previous section are shown in Fig. 10.

The suppression at very short distances is not observable in the figure because of the limited statistics of the data sample. However, the enhancement at separations of a few fm, and the suppression at scales of tens of fm is obvious. Further, since the actual droplets in the proton induced reaction are fairly large and liquidlike, this gives a good standard against which the smaller droplets formed in the heavy ion reaction can be compared. The fact that the two correlation functions are so similar is in agreement with our picture that the droplets are not just random coincidences of particles in a noninteracting gas.

We now return to comment on the significance of the reaction trajectory to the phase transition question. From both Fig. 6 and the coordinate space evolution shown in Figs. 1–3, density fluctuations play an important role in determining which nucleons will emerge in clusters. Nucleons which are scattered into low coordinate density regions tend to emerge as free particles.

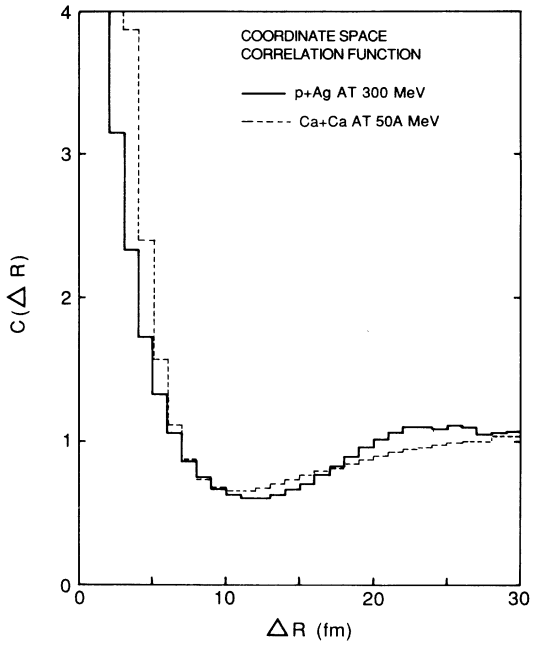

FIG. 10. Coordinate space correlation function calculated for the reaction products at an elapsed time of 150 fm/c. Two reactions at zero impact parameter are shown: p + Ag at 300 MeV and Ca + Ca at 50 MeV/nucleon.

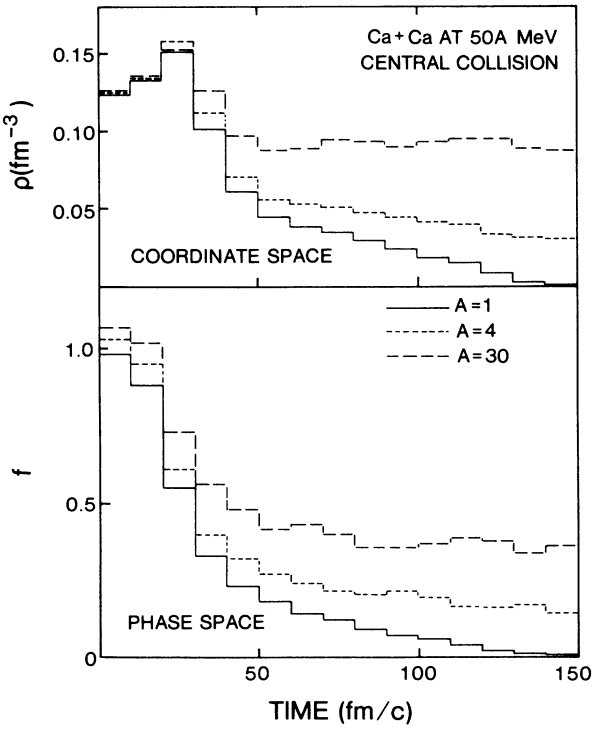

FIG. 11. Comparison of the time evolution of the local coordinate space density and phase space occupancy for Ca + Ca central collisions at 50 MeV/nucleon.

This observation is strengthened if one plots phase space density instead of coordinate space density.

The results are shown in Fig. 11, which shows the ratio of the local phase space density to the saturation density. For the proton induced reaction, the decrease in the phase space density as a function of time is slow, just as it is for the coordinate space density. The more interesting observation lies in the heavy ion reactions at the early stages of the collision. For example, at 50

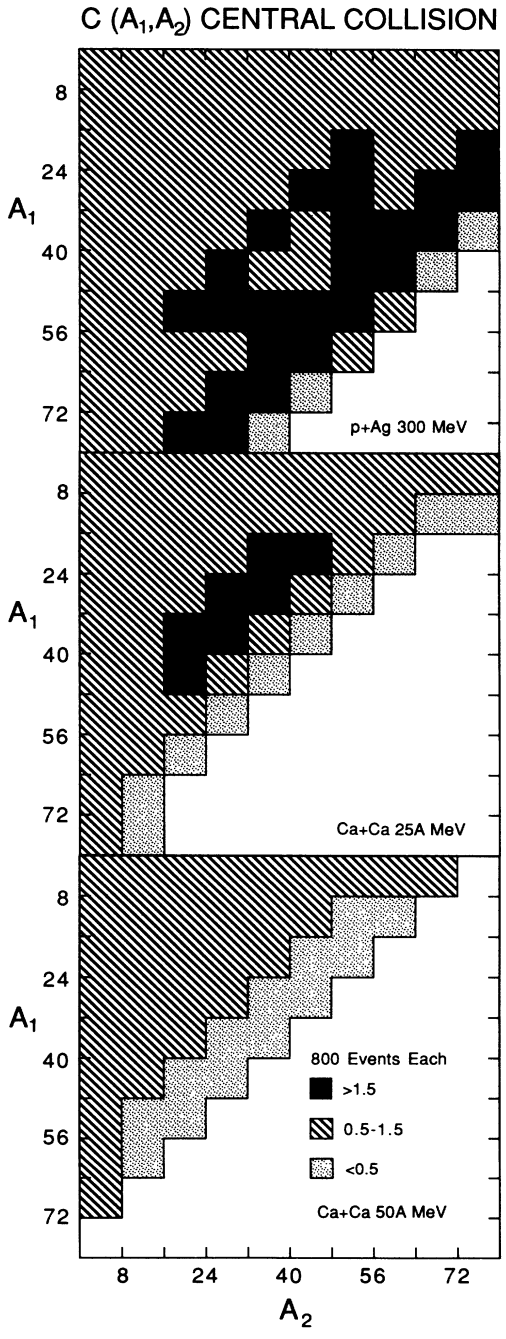

FIG. 12. Mass-mass correlation function predicted for the reactions shown in Figs. 1–3. The fragment masses are grouped in bins of 8 mass units.

TABLE I. Predicted probability for finding a pair of fragments in an event as a function of fragment masses. Each mass is binned in 8 mass units. Only fragments with mass number 80 or less are shown.

P + Ag at 300 MeV

	8	16	24	32	40	48	56	64	72	80
8	0.992	0.154	0.177	0.125	0.095	0.080	0.069	0.072	0.072	0.092
16	0.154	0.021	0.025	0.020	0.012	0.009	0.011	0.009	0.016	0.012
24	0.177	0.025	0.014	0.026	0.012	0.011	0.025	0.010	0.011	0.040
32	0.125	0.020	0.026	0.004	0.014	0.019	0.019	0.014	0.022	0.045
40	0.095	0.012	0.012	0.014	0.007	0.012	0.016	0.021	0.035	0.001
48	0.080	0.009	0.011	0.019	0.012	0.002	0.020	0.030	0.002	
56	0.069	0.011	0.025	0.019	0.016	0.020	0.005	0.004		
64	0.072	0.009	0.010	0.014	0.021	0.030	0.004			
72	0.072	0.016	0.011	0.022	0.035	0.002				
80	0.092	0.012	0.040	0.045	0.001					

Ca + Ca at 25 MeV/nucleon

	8	16	24	32	40	48	56	64	72	80
8	0.997	0.329	0.180	0.159	0.129	0.125	0.142	0.195	0.230	0.097
16	0.329	0.067	0.071	0.066	0.063	0.044	0.076	0.071	0.014	0.001
24	0.180	0.071	0.017	0.036	0.047	0.047	0.035	0.004		
32	0.159	0.066	0.036	0.029	0.045	0.037	0.002			
40	0.129	0.063	0.047	0.045	0.009	0.004				
48	0.125	0.044	0.047	0.037	0.004					
56	0.142	0.076	0.035	0.002						
64	0.195	0.071	0.004							
72	0.230	0.014								
80	0.097	0.001								

Ca + Ca at 50 MeV/nucleon

	8	16	24	32	40	48	56	64	72
8	1.000	0.615	0.366	0.272	0.225	0.160	0.100	0.060	0.014
16	0.615	0.236	0.225	0.165	0.149	0.089	0.040	0.005	
24	0.366	0.225	0.087	0.111	0.061	0.021	0.001		
32	0.272	0.165	0.111	0.027	0.025	0.002			
40	0.225	0.149	0.061	0.025	0.001				
48	0.160	0.089	0.021	0.002					
56	0.100	0.040	0.001						
64	0.060	0.005							
72	0.014								

MeV/nucleon, the coordinate space density is similar for all fragment masses at the 20–30 fm/c time step, corresponding to the period of maximum overlap. However, Fig. 11 shows that the local phase space densities of these fragments are already distinctly different. Nucleons which will ultimately emerge as free particles have already been scattered into lower density regions than those which emerge in clusters. In this sense, the formation of fragments looks somewhat like the problem of percolation in phase space, although it is the nuclear dynamics, not random association, which produces the clusters. Parenthetically, Fig. 11 also shows that the scattering mechanism for incorporating the Pauli exclusion principle is performing properly. The clusters produced in the reaction do not collapse into overbound states of high phase space density.

Hence, at intermediate energies the fluctuations produced early in the reaction tend to be propagated through it. Further, from the behavior of the mass 30 densities in Fig. 6, one observes that the average local density does not drop below some minimum value. In fact, this behavior is observed in the simulations for a wide range of fragment masses and is what is expected from the existence of the mechanical instability region. If the local density falls below a minimum value, the system breaks apart, otherwise it retracts and oscillates. In the reactions studied here, the minimum density appears to be about half nuclear matter density at low excitation energy. An important extension of these studies would be the determination of the multipolarity of the breakup modes of the excited system; this would allow a more direct comparison with the analytical investigation[16] of the phase transition region.

C. Mass correlations

From studying these three illustrative reactions, we observed the following about the reaction trajectories: At low excitation energies, the system oscillates around the coexistence region, slowly losing particles. As the excitation energy is raised, the system may enter the mechanical instability region and fragment into pieces,

depending on the energy involved.

These observations from the time evolution manifest themselves in experimental observables such as the correlation in fragment masses. We show in Table I the probability of obtaining a pair of fragments of mass A_1 and A_2. The mass bins are taken to be fairly large (8 mass units). As one would expect, the probability of obtaining a pair of light fragments is unity in all three reactions. The probability decreases as the fragment mass increases, in general. However, in the lower energy reactions, one can see an enhancement along the binary breakup line. The effect is more pronounced in the mass correlation function, defined by

$$C(A_1, A_2) = N_0 \frac{N(A_1, A_2)}{N(A_1)N(A_2)} , \tag{4.2}$$

where $N(A_1, A_2)$ is the number of coincident pairs of fragments of mass A_1 and A_2 which are produced, $N(A)$ is the number of fragments of mass A produced in the sample and N_0 is a normalization constant. As before, we construct the correlation function by the event mixing method. The predictions for the three reactions are shown in Fig. 12. There is a very large enhancement along the binary breakup line for the p + Ag reaction, the correlation function rising to about 4 for the mass bins chosen. For the 25 MeV/nucleon Ca + Ca reaction, the enhancement has been substantially reduced, at least partly reflecting the fact that one is not beginning the reaction with a large system but rather must form it during the reaction. By 50 MeV/nucleon, the enhancements have largely disappeared. Raising the bombarding energy beyond 50 MeV/nucleon continues to lower the yield of heavy fragments, but does not result in any new structure in the correlation function with the mass resolution used.

V. SUMMARY

A semiclassical model for use in the computer simulation of nuclear reactions at intermediate energy has been presented. With it, an intuitive picture of the excitation energy dependence of fragmentation processes was developed. At low energies, fragmentation was shown in the simulations to be a long time scale process involving a binary breakup. At higher excitation energies, the system breaks up into an increasingly larger number of fragments.

By using the simulations to investigate the reaction trajectories of nucleons in coordinate and phase space as they emerged as fragments from the reaction zone, it was shown that phase transition-like effects were present even in the inhomogeneous systems produced in reactions. Evidence was presented for the existence of a minimum density defining the boundary of a mechanical instability region. If the local density of a region dropped below this threshold density, the material broke up; otherwise it could recontract. While experimental determination of the boundaries of the instability region remains elusive, nevertheless it was shown that the two-particle correlation function in fragment mass should possess a clearly visible energy dependence reflecting the physics of the instability.

This work was supported in part from a grant from the Natural Sciences and Engineering Research Council of Canada.

[1]D. H. Boal, Annu. Rev. Nucl. Part. Sci. **37**, 1 (1987).
[2]J. Cugnon, Lectures given at the Cargese Summer School, 1984.
[3]G. Bertsch, in *Progress in Particle and Nuclear Physics,* edited by D. Wilkinson (Pergammon, Oxford, 1980), Vol. 4, p. 483.
[4]H. Stöcker and W. Greiner, Phys. Rep. **137**, 277 (1986).
[5]R. B. Clare and D. Strottman, Phys. Rep. **141**, 177 (1985).
[6]G. E. Beauvais, D. H. Boal, and J. C. K. Wong, Phys. Rev. C **35**, 545 (1987).
[7]G. E. Beauvais, D. H. Boal, and J. N. Glosli, Nucl. Phys. A **471**, 427c (1987).
[8]C. Gale and S. Das Gupta, Phys. Lett. **162B**, 35 (1985).
[9]J. Aichelin and H. Stöcker, Phys. Lett. B **176**, 14 (1986).
[10]C. Gregoire *et al.* Nucl. Phys. **A471**, 399c (1987).
[11]M. Blann, Annu. Rev. Nucl. Sci. **25**, 123 (1975).
[12]G. Bertsch and P. J. Siemens, Phys. Lett. **126B**, 9 (1983).
[13]D. H. Boal and A. L. Goodman, Phys. Rev. C **33**, 1690 (1986).
[14]J. A. Lopez and P. J. Siemens, Nucl. Phys. **A431**, 728 (1984).
[15]P. Bonche, S. Levit, and D. Vautherin, Nucl. Phys. **A436**, 265 (1985).
[16]C. J. Pethick and D. G. Ravenhall, in *Hadronic Matter In Collision,* edited by P. Carruthers and D. Strottman (World-Scientific, Singapore, 1986), p. 277.

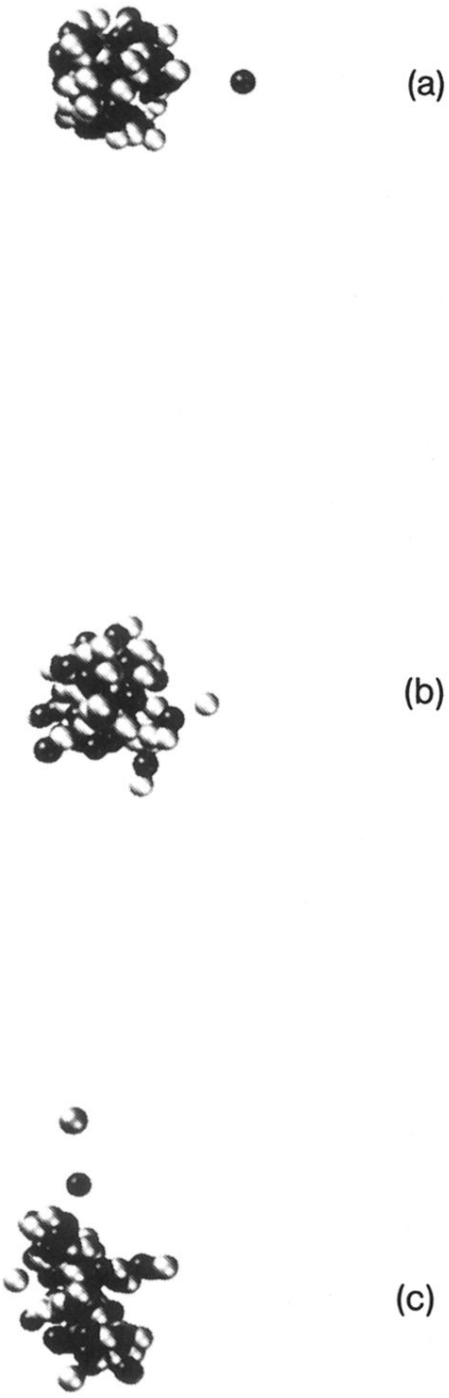

FIG. 1. Time evolution of a central p + Ag collision at 300 MeV bombarding energy. The reaction is shown at 1, 100, and 150 fm/c elapsed time. The solid spheres represent protons while the open ones are neutrons.

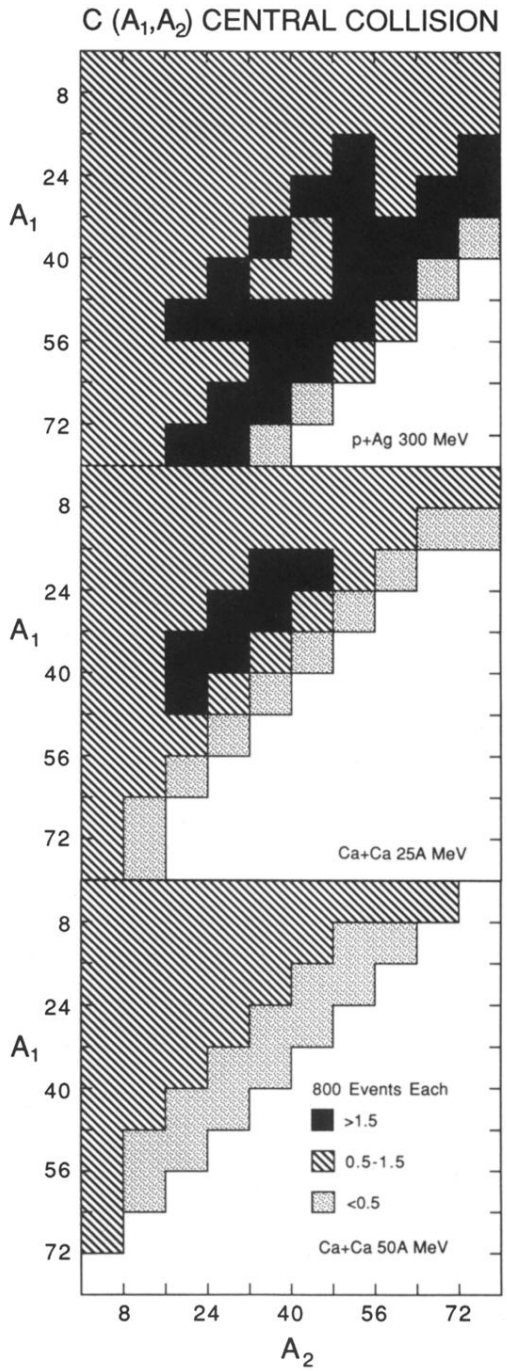

FIG. 12. Mass-mass correlation function predicted for the reactions shown in Figs. 1–3. The fragment masses are grouped in bins of 8 mass units.

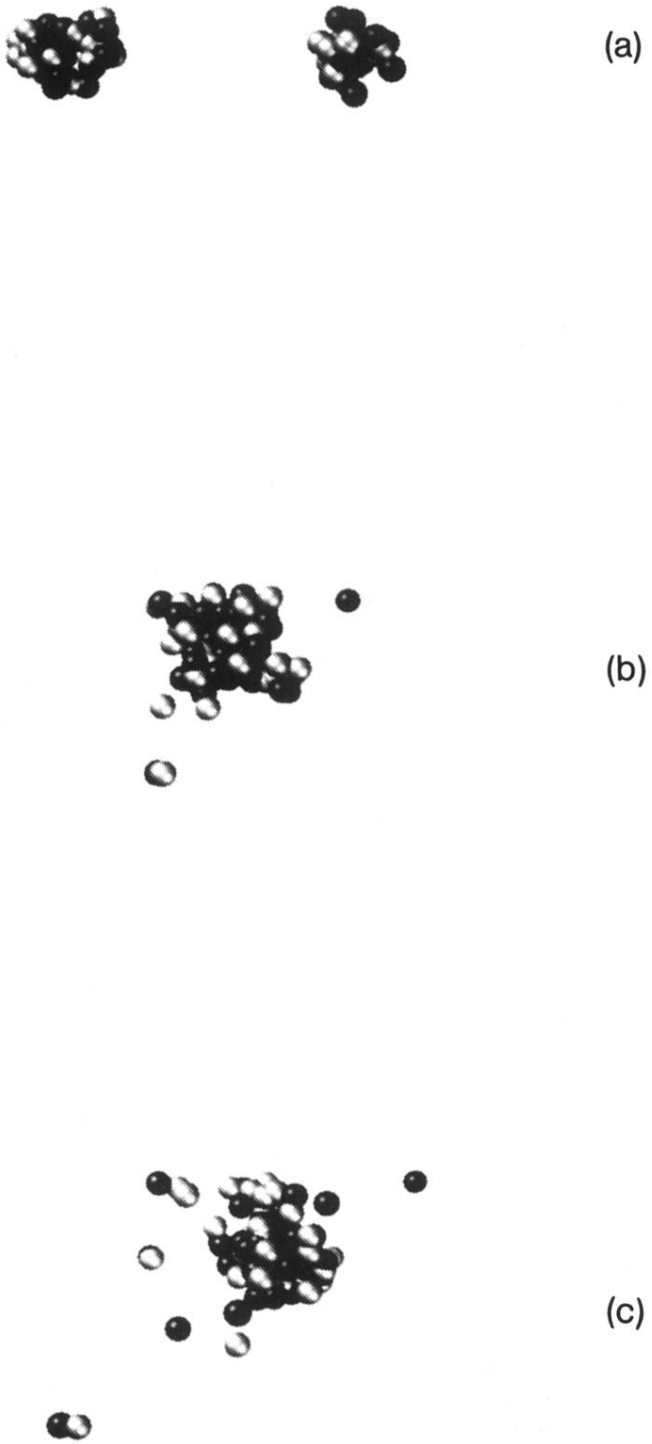

FIG. 2. Time evolution of a central Ca + Ca collision at 25 MeV/nucleon bombarding energy. Same representation as Fig. 1.

FIG. 3. Time evolution of a central Ca + Ca collision at 50 MeV/nuclon bombarding energy. Same representation as Fig. 1.

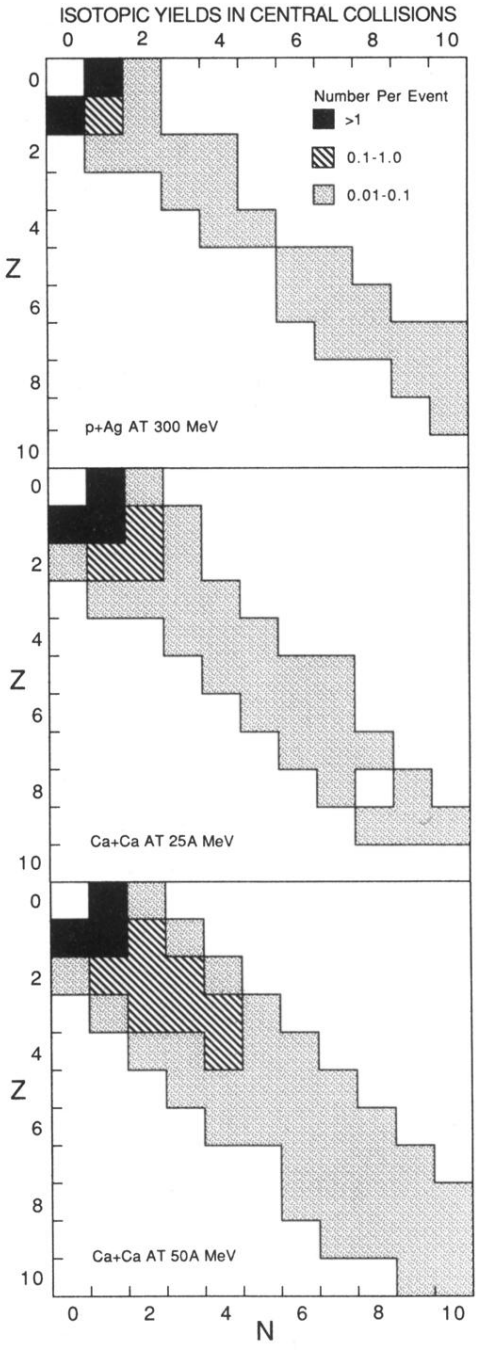

FIG. 4. Isotopic yields in the light to medium mass fragment range for the reactions shown in Figs. 1–3. The yields are given as the number of fragments of a given Z,N per event.